J. Fluid Mech. (1967), *vol.* 28, *part* 3, *pp.* 501–512
Printed in Great Britain

The vortex wakes of vibrating cylinders at low Reynolds numbers

By G. H. KOOPMANN
U.S. Naval Research Laboratory, Washington, D.C.

(Received 14 April 1966 and in revised form 19 July 1966)

The effect of the transverse motion of a cylinder on its natural vortex wake is examined at various driving frequencies giving special attention to the change in wake geometry along the span. Conditions are established for which the vortex wake frequency is controlled by the driving frequency of the cylinder.

1. Introduction

This paper presents the results of an experimental investigation which was conducted to determine what effect the forced vibration of a circular cylinder in fluid flow has on the resultant wake geometry at low Reynolds numbers. The study was undertaken for the purpose of better understanding the mechanics of a vortex-induced vibration by closely examining the interplay between a vibrating body and its vortex wake. The oscillating flow fields in the wakes of both blunt and streamlined bodies have been examined and classified by several investigators. However, little is known about the changes that occur in the geometry of the wake pattern when the body vibrates at the frequency of the oscillating wake. Of particular interest is the change in the wake pattern along the span of the vibrating body. The motion of the trailing edge appears to organize the phase of the fluctuating wake over a greater length of the span, thus permitting a greater instantaneous lift force on the body. This same motion can also control the frequency of the oscillating wake over a limited range, a phenomenon known as 'locking-in'.

2. Early investigations and observations

In 1878, Strouhal published his basic work concerning Aeolian tones. In Strouhal's experiments, a vertical wire held firmly by a suitable support was spun around a parallel axis at a uniform velocity. The frequency of the Aeolian tone resulting from the motion of the wire through the air was found to vary only with wire diameter and speed of motion and was independent of length and tension of the wire. It was also observed that when the Aeolian tones coincided with one of the natural tones of the wire, which was free to vibrate, the sound was greatly reinforced. A year later Lord Rayleigh (1879), while observing a violin string vibrating due to the impact of the wind, discovered that the vibration of the string took place in a plane normal to the direction of the wind, rather than in a plane contained by the wind as was the previous opinion. In 1908, Bénard correlated the

musical notes studies by Strouhal with two nearly parallel rows of nearly equal-spaced vortices behind a cylinder, that is, with a so-called vortex street. This then was the beginning for understanding the fluid mechanics responsible for Aeolian tones. When the mechanics of the structure must also be included in the analysis, as in the case of the violin string, the resulting vibration is considered to be vortex-induced.

3. Recent investigations and observations

In 1952, Gongwer published a paper on singing vanes in water. His work definitely established that the induced vibration of the vanes under study was caused by the shedding of vortex streets. A proportionality between frequency and speed closely followed the Strouhal number. Gongwer also noted that each note held at a nearly constant frequency over a short range of speed. This seemed to indicate that the vortex street geometry was influenced by the vibrating segments of the vanes, i.e. a 'locking-in' condition existed. Brown (1959), during a wind tunnel study, found it possible to influence the frequency of a vortex wake being shed behind a cylinder by introducing a sound field in the test section. By varying the frequency of the sound field around the natural frequency of the wake, it was possible to control the resulting wake frequency over a range of 0·8–1·2 times the natural frequency. In 1962, Powell & Shulman also observed this 'locking-in' effect during an experiment with Aeolian tones. As the wind velocity was steadily increased, the tone increased proportionately, until suddenly at some point the tone took on a resonant frequency of the wire, became steady and intense, and held over about a 10 % increase in speed.

Wehrmann (1965) investigated the influence that a vibrating cylinder has on its vortex wake at low Reynolds numbers. He found that driving the cylinder at the shedding frequency of the vortices reduced the intensity of the velocity fluctuations in the wake by a substantial amount. Ferguson (1965) found that the motion of a vortex-excited cylinder causes a narrowing of the wake when the vortices are shed at the system's resonant frequency.

4. Experimental apparatus

Wind tunnel

The test facility is a 3×3 in. low turbulence tunnel designed especially to meet the requirements of the experiments. The turbulence level is about 0·2 %. The tunnel entrance is fitted with five 80-mesh screens and is followed by a settling chamber. The entrance jet, which has a 20:1 contraction ratio, provides a velocity profile which is flat to within 1 % at the test section. The profile for the jet wall was obtained from the theoretical curves of Smith & Wang (1944). The test sections are constructed of clear lucite and vary in length from 10 to 24 in. Velocities in the test section range from 1 ft./sec to 60 ft./sec. The diffuser has an 8° divergence angle and is followed by two 6 in. contrarotating fans which are driven by a synchronous motor working through a speed reducer. The fan speed is monitored with a stroboscope.

Velocity measurements

Velocity measurements in the test section were made with a calibrated Prandtl-type pitot tube measuring $\frac{1}{16}$ in. in diameter. The tube could be moved in a plane normal to the flow by means of an adjustable stand. The differential pressures were read with a slanted tube manometer operating on a null balance principle. The device was nulled by moving a well in a vertical plane by means of a precision lead screw from which direct readings were taken. A total magnification factor of $\times$ 1000 was achieved by employing a simple optical system to project an image of the meniscus on an appropriate gridwork. By using this technique, it was possible to read pressure changes to within $\pm$ 0·0005 in. of alcohol.

Flow studies

The wind tunnel has provisions for conducting flow studies using smoke as an indicator. The entrance jet can be fitted with a slender airfoil having a slotted trailing edge that produces a thin uniform sheet of smoke a few mils thick extending the width of the tunnel. The smoke sheet remains laminar and flat provided that there is no relative velocity between the jet and the flow over the airfoil. Smoke is generated using a simple apparatus which forces the burning of tobacco with compressed air. The smoke is cooled and filtered before it reaches the test section, thereby greatly reducing the amount of tars and stains that normally collect in both the apparatus itself and on the test pieces. At low tunnel velocities, helium is added to the smoke to balance the effect of gravity.

Street frequency measurement

The sensor used to detect the velocity fluctuation in the wake of the test cylinder was a 0·15 mil tungsten hot wire. The probe holding the wire was mounted to an adjustable stand which allowed for transversing in planes normal to the flow in a region extending 2 in. behind the cylinder. A measuring microscope was used to locate the position of the hot wire relative to the test cylinder. Readings were accurate to about 5 mils. The frequencies of the periodic fluctuations were obtained by observing Lissajous figures on an oscilloscope. The reference frequency was taken from a Hewlett–Packard Model 200 D Audio Oscillator which in turn was checked by a Hewlett–Packard Model 521 ER Electronic Counter.

Cylinders and support mechanism

The cylinders used in the experiment were highly polished drill rods ranging in size from 0·094 to 0·156 in. and extending the width of the test section. The dimensional tolerances were less than 1 mil. The cylinders were supported by a Y-shaped aluminium yoke which straddled the test section (shown in figure 1, plate 1). The yoke was driven in a plane normal to the flow by a 5 lb. Vibrasonics Model VS-5 Shaker supplied by a 75 W McIntosh Power Amplifier. The driving signal was provided by a Hewlett–Packard Model 200 D Audio Oscillator which was monitored by a Hewlett–Packard Model 521 ER Electronic Counter.

Measurements for the calculation of displacement amplitude were obtained from a calibrated Massa Model 5B Accelerometer which was mounted directly to the centre of the yoke (figure 2).

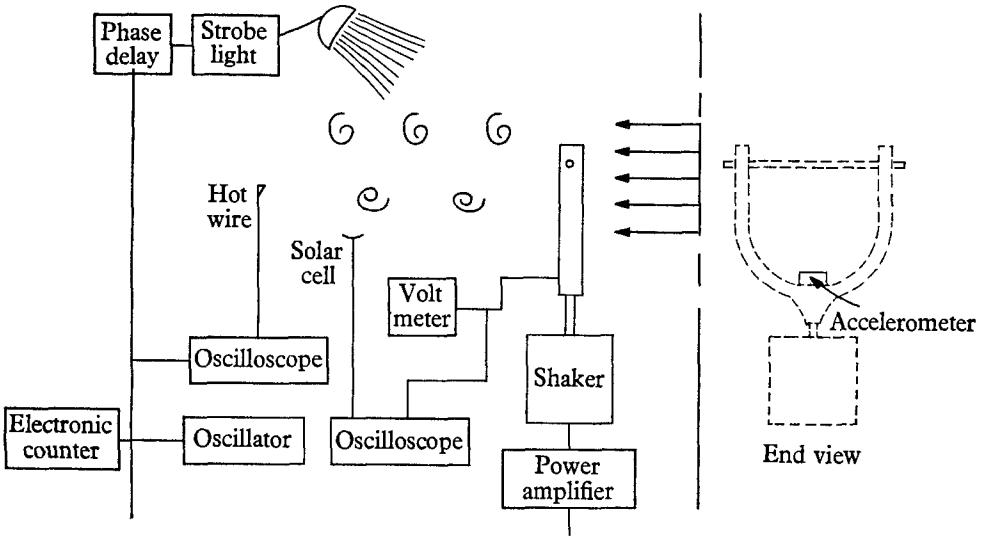

FIGURE 2. Line diagram of the apparatus.

Photography

Pictures of the vortex wake were first taken with the film plane parallel to the flow but normal to the axis of the cylinder, and second with the film plane parallel to the plane contained by both the free-stream and the axis of the cylinder. Since the smoke jet could be pivoted 90 degrees, the smoke sheet was always photographed parallel to the film plane. A 35 mm Nikon camera and a Graphic view camera with a 4×5 Polaroid film pack were both used to obtain photographs for experimental purposes. Light was provided by two General Radio Strobotacs with one driving the other. The driver Strobotac shared the audio oscillator signal with the cylinder shaker, but was equipped with a flash delay for examining the wake patterns of various points in the cylinder travel. This phase difference was accurately measured by comparing the signal of a solar cell which was activated by the light flash with the signal of the accelerometer which was mounted to the yoke.

5. Preliminary work

Before experimental data could be received from the new tunnel with any degree of confidence, it was necessary to determine its performance characteristics at the appropriate wind velocities. After measurements of both the turbulence level and the velocity profile were obtained and were found to be of an acceptable level, it was decided to conduct a series of experiments which would allow a comparison of the results to be made with an already existing and well established piece of work. The work of Roshko (1954) was chosen for this purpose since part

of it included a study of vortex streets shedding behind cylinders at low Reynolds numbers. Roshko had experimentally established a relationship describing the Strouhal number as a function of Reynolds number up to $Re = 1400$. Additional work by Etkin, Korbacher & Keefe (1956) has extended this relationship to $Re = 200{,}000$. This set of experiments appeared to be adaptable to the new tunnel. A series of tests were performed on cylinders with diameters ranging from 0·012 to 0·125 in. A comparison of the results showed an agreement to within 5 % of Roshko's best fit curve indicating that subsequent experimental data could be accepted with confidence.

Several interdependent factors were found to limit the possible range of Reynolds numbers. These consisted of the maximum tunnel blockage ratio, the frequency limit of the stroboscopic light, the power output of the shaker, and the stability range of the smoke sheet. As a compromise of these limitations, it was decided to conduct experiments on three cylinders in the characteristic Reynolds ranges of 100, 200 and 300, i.e. the stable range, the transition range, and the irregular range.

6. The appearance and structure of vortex wakes at natural shedding

The first series of experiments was directed towards examining both the two-dimensional and the three-dimensional appearance of the vortex wake patterns at natural shedding conditions, i.e. with no vibration of the cylinder.

A cross-sectional view of the vortex wake (figure 3, plate 2) indicates a shedding mechanism similar to the one explained by Goldstein (1938). The boundary layer separates from each side of the cylinder and continues on in the main flow as a free vortex layer which separates the fluid in the wake from the main flow. Under this unstable condition, the free vortex layer begins to roll up in such a way that a vortex is formed at its end. The vortex is then shed alternately with the one on the opposite side and continues its winding up motion as it moves downstream. This asymmetrical arrangement of vortices is accompanied by an alternating pressure which causes the cylinder to experience an alternating lift force in a direction perpendicular to the flow.

The three-dimensional pattern of a vortex wake as seen from above is given in figure 4, plate 2. A similar wake pattern has been observed by Berger (1964*a*, *b*). The vortex filaments are straight but inclined to the axis of the cylinder. The point on the cylinder at which the boundary layer first separates determines the direction of the slant angle of the filaments. The top view looking downstream shows a counter-clockwise slant angle when the separation point begins on the right end of the cylinder and proceeds to the left. The opposite holds true for the reverse case. The rate of travel of the separation point along the cylinder is somewhat dependent upon the normal alignment of the cylinder relative to the free stream. A slight turn of the cylinder in a plane containing the flow and the cylinder will cause the vortex filament lines to slant in the opposite direction. When the cylinder is carefully positioned normal to the flow, an unstable condition can be set up. The separation point originates at the centre of the cylinder and proceeds toward the ends, giving a curved pattern of the vortex filaments. During

this condition, the curved filaments occasionally straighten and take on either slant angle. After a period of time, a sudden shift causes the filament lines to return to their original curved shape.

7. The appearance of the vortex wake with the cylinder vibrating at the natural shedding frequency

The second series of experiments was performed to determine what effect the transverse motion of the cylinder vibrating in its rigid body mode has on the resultant wake geometry. The driving frequency in this case was identical to the natural shedding frequency of the vortex wake which formed while holding the cylinder stationary. The scheme used to impose this condition was quite simple. The apparent motion of the vortices was stopped by selecting an appropriate driving signal frequency for the strobelight. This same signal was then shared by the electronic shaker used to drive the cylinder.

As the displacement amplitude of the cylinder was slowly increased, a certain threshold amplitude was reached where the vortex street exhibited a dramatic change. The vortex filaments, which before vibrating had been shedding in a slanted direction, suddenly jumped to align themselves parallel to the cylinder. This is illustrated in figure 5, plate 3. It can be seen that the initial vortex filament is straight along most of the span of the cylinder. This configuration was very stable and even maintained itself during an occasional upstream disturbance. The curved ends of the filaments are due to the retarded flow in the boundary layer along the wall of the tunnel. This same effect also explains the gradual increase in curvature of the filaments as they progress downstream. An increase in displacement amplitude beyond the threshold yielded no noticeable change in the geometry when viewed from above.

A cross-sectional view of the vortex wake behind the cylinder vibrating at the natural shedding frequency is shown in figure 6, plate 3. The motion of the cylinder tends to decrease the lateral spacing of the vortices while the longitudinal spacing remained unchanged.

A phase delay in the strobelight circuit allowed for close examination of the early vortex wake at various points of the cylinder's travel. Figure 7, plate 4 shows the formation of the early vortex wake when the cylinder has reached its lowest point of travel. The vortex layer on the bottom side has just separated from the cylinder.

The critical vibration displacement for which the vortex filaments became aligned parallel to the cylinder was determined for each range of Reynolds numbers. A first set of points was obtained by observing the smoke patterns of the vortex filaments while the vibrational displacement of the cylinder was slowly increased. The critical displacement point was considered to be reached when the vortex filaments changed from their unstable slanted configuration and became stable and parallel to the cylinder. A second method was used to check the above technique. Two hot wires were placed downstream equidistant from the cylinder about $1\frac{1}{2}$ in. apart. The phase of the signals from the hot wires was read on an oscilloscope in the form of a Lissajous figure. With no cylinder vibration, the

phase was unsteady and changed constantly. A critical displacement point was considered to be reached when the signals from the hot wires were steady and in phase. Both methods yielded the same results. For all three ranges of Reynolds numbers, a vibrational displacement of about 10% of the cylinder diameter would cause the vortex filaments to align themselves parallel to the cylinder.

The induced street velocity in the upstream direction was calculated for both the vibrating and non-vibrating case. Since the product of the measured street wavelength and the corresponding frequency gave the downstream velocity, the induced street velocity was simply the difference of this quantity and the free stream velocity. Results indicated that the induced street velocities were the same for both cases.

8. The appearance of the vortex wake with the cylinder vibrating at a frequency other than the natural shedding frequency

The third set of experiments was conducted to observe the changes that occur in the wake geometry of a cylinder that is forced to vibrate at frequencies varied around the natural vortex frequency. Of particular interest were the conditions for which the shedding frequency continued to be identical to the driving frequency, i.e. conditions for which the vortex street was 'locked-in'. This would help to explain the interplay between a structure and its vortex wake that causes the structure to vibrate at a nearly constant normal mode frequency while the velocity field around the structure changes over a certain range.

The range over which the vortex street frequency was controlled by the motion of the driver cylinder was determined by the following method. Since small changes in tunnel velocities were difficult to measure at low levels, the driving frequency was varied while the velocity was held constant for each set of Reynolds numbers. The street frequency was measured with a hot wire which was placed downstream in the wake of the cylinder. A Lissajous figure was observed in order to judge when the signals from the hot wire and the driver oscillator were of the same frequency. The vortex street was considered to be 'locked-in' when the Lissajous figure appeared as a steady single loop. The vibration of the cylinder was started at the natural shedding frequency. After a fixed displacement amplitude was chosen, the driving frequency was slowly varied until the stable single pattern of the Lissajous figure vanished, thus indicating that an end point had been reached. The results are given in figure 8.

Both the upper and lower frequency limits appear to be similar functions of the displacement/diameter ratio. With the exception of the curve for $Re = 100$, the upper frequency limit points corresponding to displacement/diameter ratios above 25% were limited by the power output of the electronic shaker.

Several photographs were taken of the 'locked-in' vortex street at both the upper and lower frequency limits. For both cases, the vortex filaments aligned themselves parallel to the cylinder. A comparison of the street geometry at the upper and lower frequency limits is shown in figure 9, plate 5. A vibration of the cylinder at the upper frequency limit caused the street to be compressed, i.e. the longitudinal spacing between the vortex filaments was decreased. Similarly, a vibration at the lower frequency limit caused the street to be expanded.

The cross-sectional views of the vortex filaments at the upper and lower frequency limits are shown in figure 10, plate 6. It was surprising to find that the two totally different wake patterns were both stable at the same free stream velocity. The flow configuration at the lower frequency limit is an especially radical departure from the more common spacing arrangement observed during natural shedding conditions. Of particular notice is the reduction in lateral spacing of the rows which almost makes them appear to be collinear. The flow configurations at the upper frequency limit offered some explanation of how the

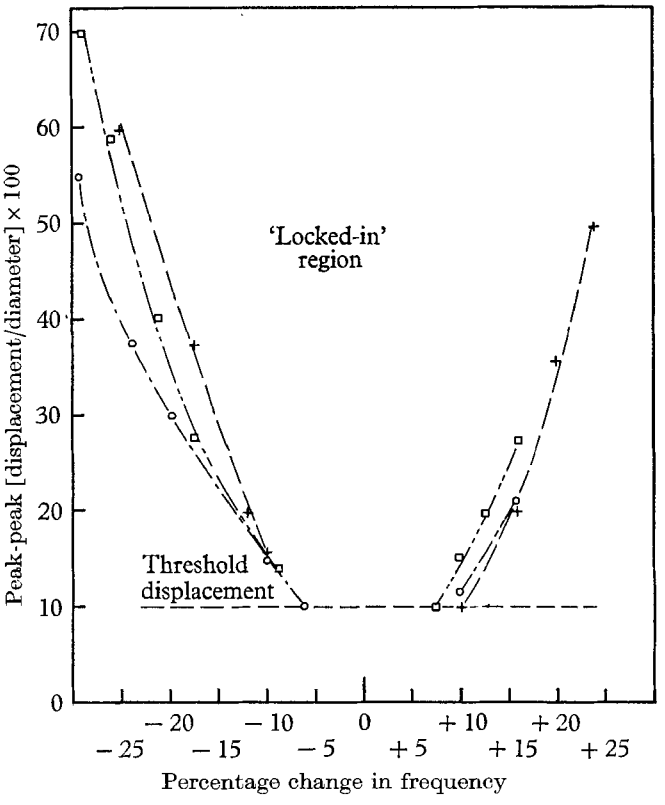

FIGURE 8. Regions over which the cylinder motion controls the shedding frequency of its vortex wake. ——, Re = 100; —·—·—, Re = 200; —·—, Re = 300.

vortex street becomes unlocked when the cylinder is driven at a frequency above the upper limit. It can be seen from the photograph that the vortex spiral becomes diffused into a turbulent wake at a certain point downstream. For this particular set of conditions, the breakdown point occurred about three street lengths from the cylinder. As the upper frequency limit was slowly approached, the breakdown point travelled upstream toward the cylinder until the entire wake was filled with turbulence. The vortex street was then unlocked.

The induced velocity of the vortex street in the upstream direction was calculated from measurements taken from photographs at the upper and lower frequency limits. A typical relation between street velocity and frequency within

the 'locked-in' region is shown in figure 11. In general the induced street velocity varied directly with frequency; thus the street velocity corresponding to the upper frequency limit was higher than the street velocity at natural shedding conditions and vice versa.

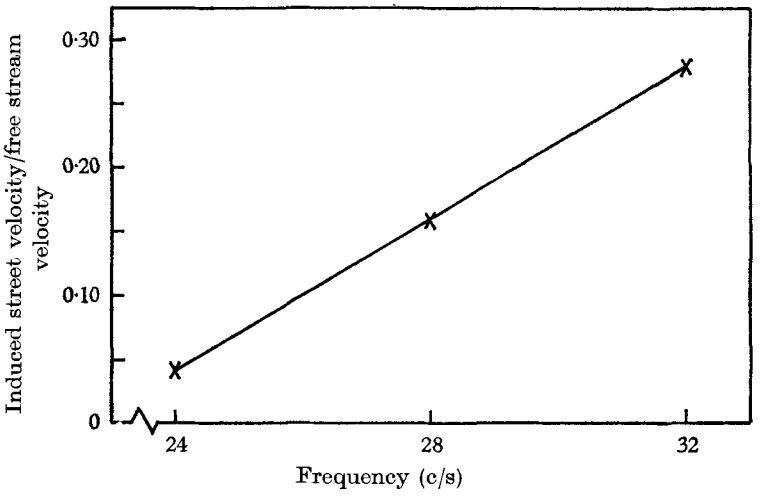

FIGURE 11. Relationship between frequency and induced street velocity within the 'locked-in' region. $Re = 200$.

9. Vortex strength

The clarity of the streaklines marking the spirals within the vortices provided a means for evaluating the strength of each vortex within the street. The streaklines give a time and space history of the path followed by a fluid particle that is initially entrained in the region of concentrated vorticity in the immediate wake of the cylinder. If the streaklines are considered to be composed of a continual chain of fluid particles which initially move in a direction parallel to the free stream, then the subsequent deformation of this chain as observed in the still photographs permits the angular displacement of a fluid particle to be determined over some given time. To perform such a kinematical analysis each vortex is treated as an isolated vortex, i.e. it neither influences or is influenced by other nearby vortices. It is further assumed that each vortex originates in the immediate wake of the cylinder at time $t = 0$ and grows by a diffusion process as it proceeds downstream. A model which accommodates an analysis of this type is found in the Hamel–Oseen vortex, since it accounts for the effects of viscosity in the fluid. The distributions of vorticity ζ and angular velocity ω at time t and radius r are given by

$$\zeta = \frac{k}{4\pi\nu t}\exp\{-r^2/4\nu t\}, \tag{1}$$

$$\omega = \frac{k}{2\pi r^2}[1-\exp\{-r^2/4\nu t\}], \tag{2}$$

where k is the vortex strength and ν the kinematic viscosity. In this model, the particle flow is symmetric about the centre axis and excludes flow in the radial

direction. As the vortex grows in time, the centre core, which moves as a slug of fluid, steadily grows in radius while its angular velocity decreases. An expression giving the deformation of an initially radial line of fluid particles within the vortex over a known time t can be obtained by integrating (2) in the form

$$\theta = \frac{k}{2\pi r^2}\int_0^t [1-\exp\{-r^2/4\nu t\}]dt. \tag{3}$$

The integration of this expression was performed on a digital computer with the integration constants for t chosen to correspond to the downstream time of each successive vortex. The results of the integration for each given time yielded functions having geometrical patterns which closely resembled the vortex streaklines observed in the photographs. The analysis presented here is based upon the assumption that the streaklines trace the progressive deformation of an initially horizontal radial line of particles within the vortex. The strength of each vortex

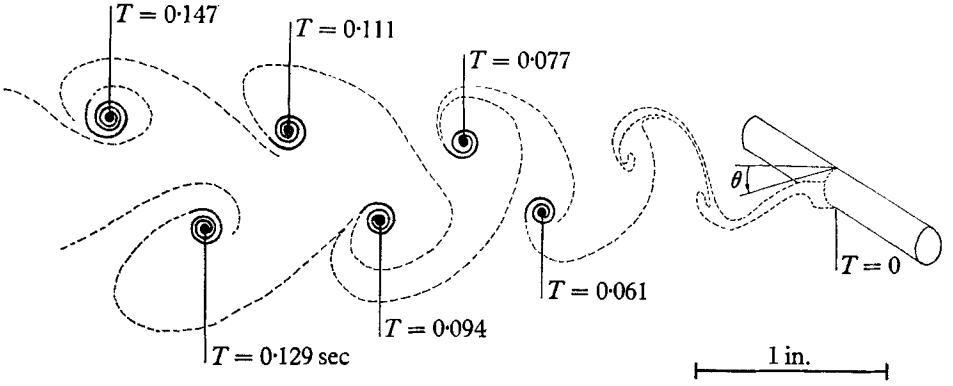

FIGURE 12. Vortex wake pattern obtained by replacing observed vortices with vortex model. Re = 200. Solid lines represent geometrical pattern given by the function

$$\theta = \frac{k}{2\pi r^2}\int_0^T [1-\exp\{-r^2/4\nu t\}]dt.$$

Empirical value for k = 4·71 in.²/sec.

was determined by choosing an average value for k which produced a set of functions from (3) having the closest possible geometrical similarity to that of the vortices observed in the photographs. For purposes of fitting the model, the first radial point was chosen to lie on the periphery of the vortex core which appeared as a solid slug of smoke in the photographs. The radius of the black dots shown in figure 12 has a dimension which corresponds to this measurement from the photograph. The integration limits extended from the edge of this vortex core to the region of maximum angular velocity. To orient the angular rotation of the first radial point, a horizontal reference line was chosen at t = 0 with the angles being measured down from the horizontal for the upper rows and up from the horizontal for the bottom rows. A proper fit of the vortex model (shown in figure 12) with the observed vortex street (shown in figure 3) gave a value for the vortex strength.

$$k = 4{\cdot}71\,\text{in.}^2/\text{sec}.$$

This value for k can be compared with the results of other investigators by using a dimensionless characteristic quantity of the flow

$$\Lambda = K/U_\infty^2,$$

where U_∞ is the free stream velocity of the fluid and K is the initial circulation/unit time in the separated flow which is given as the product of the vortex strength and the street frequency. Berger (1964*a*, *b*), in an experimental analysis using hot-wire measurements, obtained a value of

$$\Lambda = 0{\cdot}39.$$

Birkhoff & Zarantonello (1957) empirically determined that the value should be

$$\Lambda \simeq 0{\cdot}40.$$

Using the value of $k = 4{\cdot}71\,\text{in.}^2/\text{sec}$ obtained by the above analysis gives

$$\Lambda = 0{\cdot}32,$$

which is in fair agreement with the other two values.

10. Vibration and the Strouhal number

The dimensionless Strouhal number relates the parameters of frequency, dimension and velocity. For a circular cylinder, these parameters are usually chosen as the street frequency, cylinder diameter, and free-stream velocity. When the cylinder is allowed to vibrate transverse to the flow, it would seem appropriate to correct the dimensional parameter by adding to it the total amplitude of vibration. This treatment was suggested by Landwebber (1942) on the basis that the normal width of the vortex street would be increased by the total amplitude of vibration since the vortex was found to shed at the end of the oscillation cycle. The photographs taken during vibrations at the natural shedding frequency revealed an entirely different geometrical arrangement than expected (figure 6). The effect of the vibration was to decrease rather than increase the width of the vortex street while the longitudinal spacing remained unchanged. When writing the Strouhal number as a function of Reynolds number for these vibrating conditions ($Re < 300$), the problem becomes one of choosing boundaries which would include all the possible points. As a rough approximation for the boundary lines, the $\pm 25\,\%$ frequency variation noted during the 'locked-in' condition provides a basis for describing the Strouhal frequency. Using this variation as the frequency and holding the velocity and dimension parameters constant, the Strouhal number would then have a possible range of $\pm 25\%$ for some constant Reynolds number. This rather broad boundary should contain all the points covering the S–R relationships for the cases where the cylinder is allowed to vibrate.

11. Summary of results

Above a determined threshold amplitude, the transverse vibration of a cylinder driven at the natural frequency of its vortex wake induces coherence of the separation points along its span.

The upper and lower range of frequencies for which the shedding frequency is controlled by the driving frequency of the cylinder are amplitude and, to some extent, Reynolds numbers dependent.

As the upper frequency limit is approached, the transition point where the laminar wake becomes turbulent moves toward the cylinder and eventually becomes attached.

The geometry of the vortex wake is altered appreciably by the motion of the cylinder which, in general, causes a reduction in the lateral spacing of the wake vortices.

A measure of the vortex strength can be obtained by replacing each vortex in the street with a similar geometrical vortex model of the Hamel–Oseen type.

The author is greatly indebted to his colleague, Charles W. Votaw, for much valuable help and encouragement throughout the course of this work. The author also wishes to thank Dr B. H. Atabeck of Catholic University for his helpful advice, and L. R. Dragonette for his helpful work in preparing the computer program.

REFERENCES

BÉNARD, H. 1908 *Comptes Rendus*, **147**, 839–42, 970.

BERGER, E. 1964*a* Presented at I.U.T.A.M. Symposium at Ann Arbor, Michigan.

BERGER, E. 1964*b*. *Z. Flugwiss.* **12**, 41–59.

BIRKHOFF, G. & ZARRANTONELLO, E. 1957 *Jets, Wakes and Cavities.* New York: Academic Press.

BROWN, F. N. M. 1959 *University of Texas, Sixth Midwestern Conference on Fluid Mechanics*, pp. 331–49.

ETKIN, B., KORBACHER, G. K. & KEEFE, R. T. 1956 *UTIA Rept.* no. 39.

FERGUSON, N. 1965 Master Thesis, Department of Mechanical Engineering, The University of British Columbia, Canada.

GOLDSTEIN, S. 1938 *Modern Developments in Fluid Dynamics*, Vol. II. Oxford University Press.

GONGWER, C. A. 1952 *J. Appl. Mech.* pp. 432–8.

LANDWEBBER, L. 1942 *DTMB Rept.* p. 485.

POWELL, A. & SHULMAN, A. 1962 *J. Acoust. Soc. Am.* **34**, 1146–7.

RAYLEIGH, LORD 1879 *Phil. Mag.* **7**, p. 149.

ROSHKO, A. 1954 *NACA Rept.* p. 1191.

SMITH, R. & WANG, C. 1944 *J. Aero. Sci.* pp. 356–60.

STROUHAL, V. 1878 *Weid. Ann.* **5**, 216.

WEHRMANN, O. H. 1965 *Phys. Fluids*, **8**, 760–1.

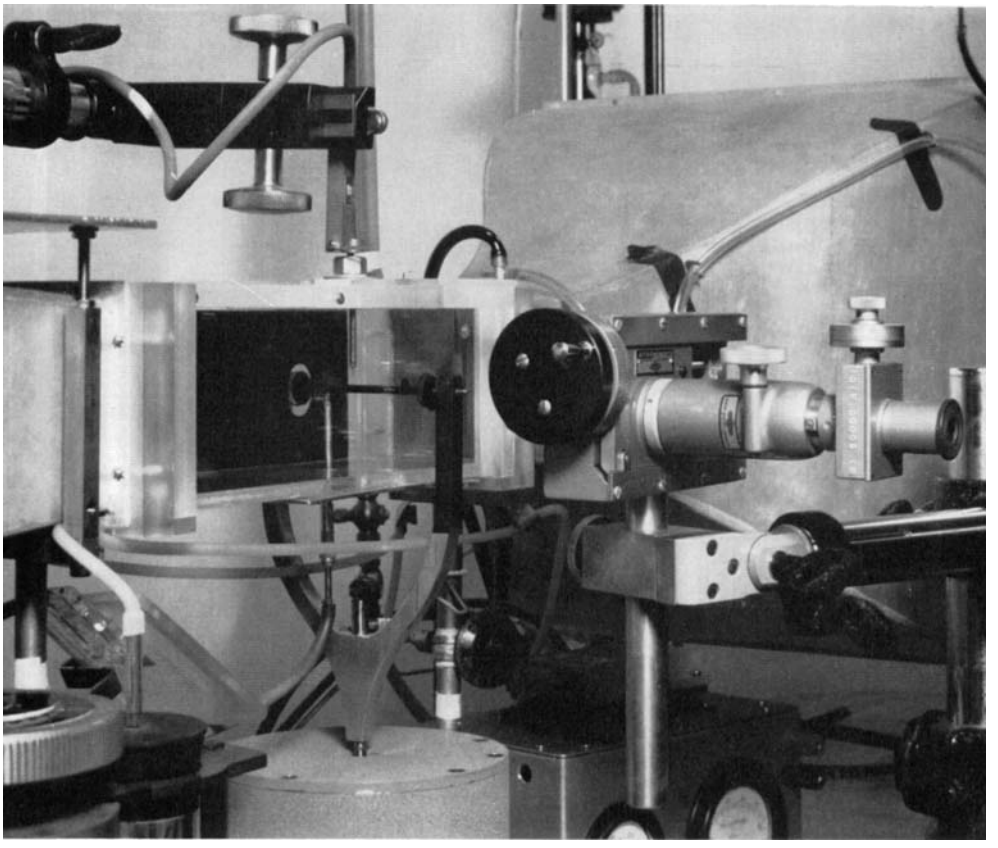

FIGURE 1. Test section and cylinder support.

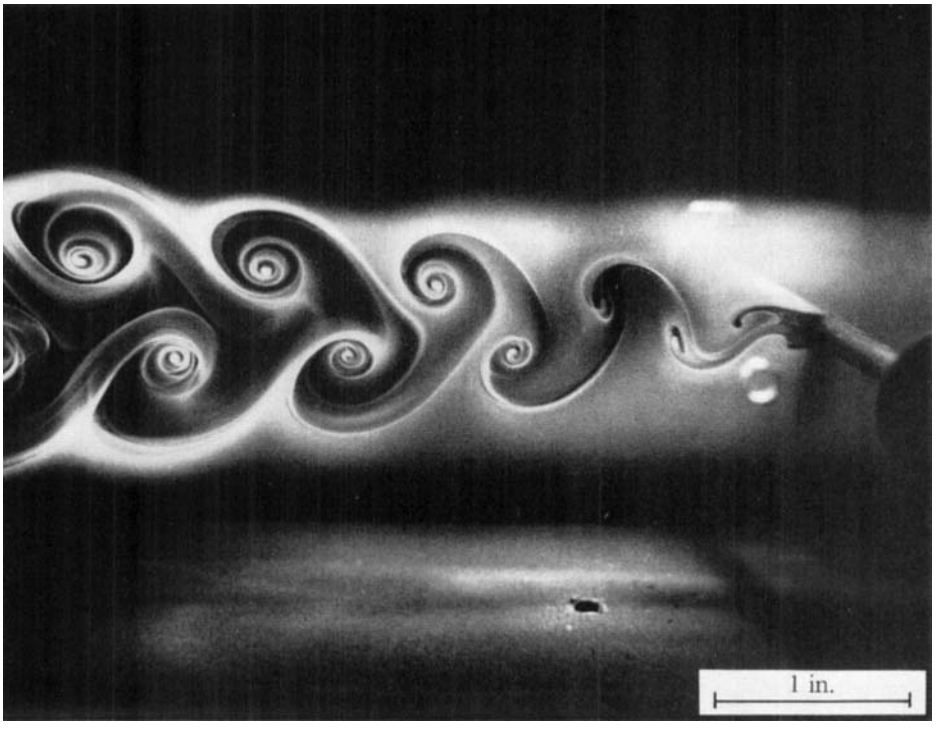

FIGURE 3. Cross-sectional view of vortex wake shedding from stationary cylinder ($Re = 200$, frequency = 28).

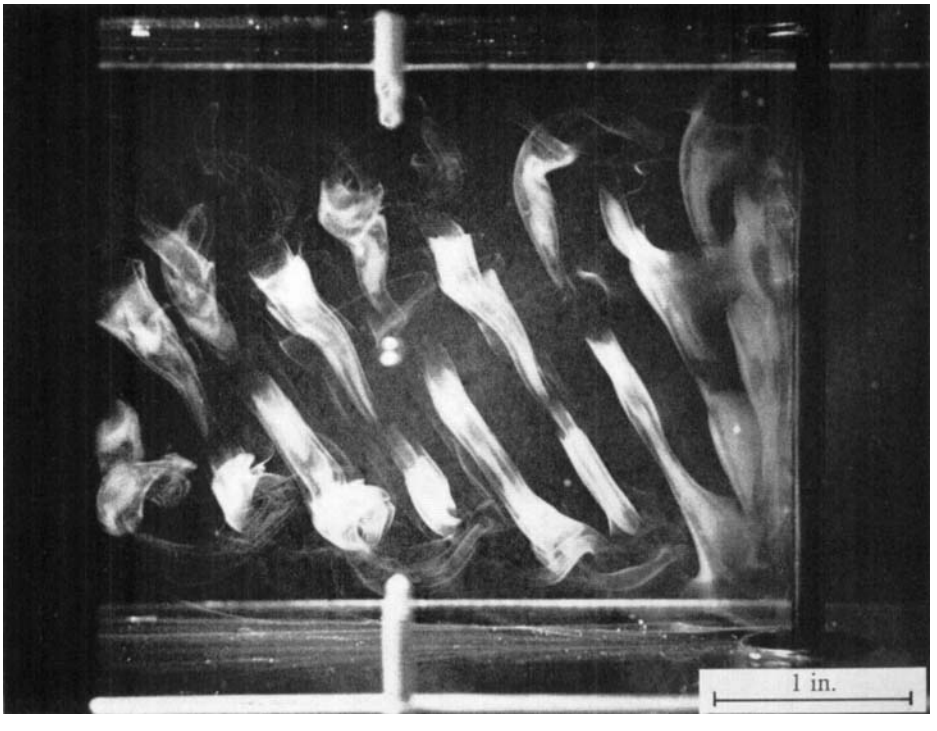

FIGURE 4. Top view of the inclined filaments of a vortex wake shedding from a stationary cylinder ($Re = 200$, frequency = 28).

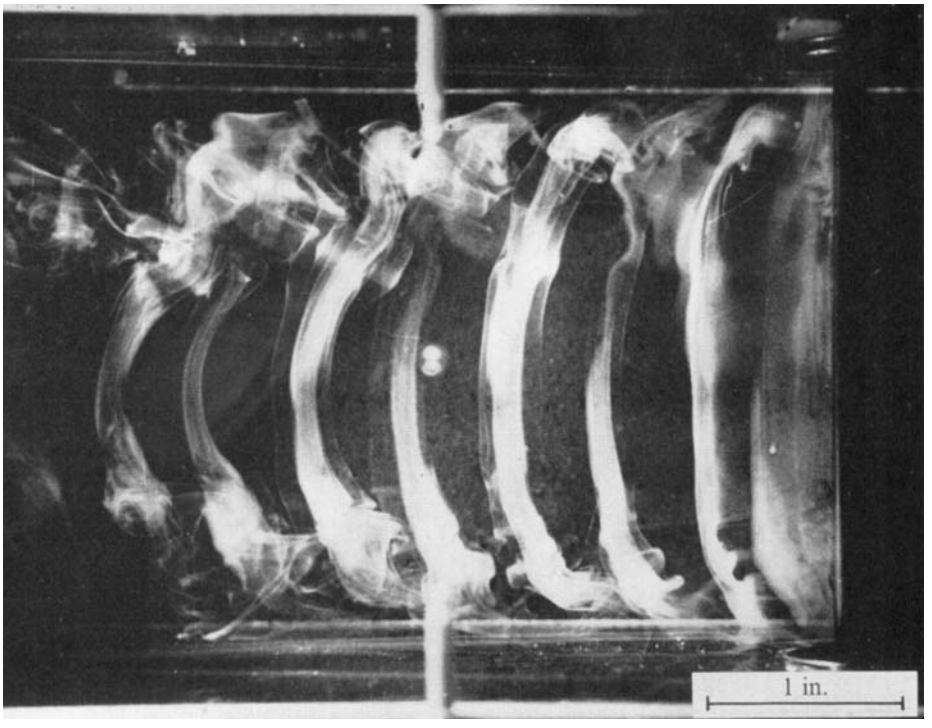

FIGURE 5. Top view of the filaments of a vortex wake shedding from a vibrating cylinder (Re = 200, cylinder frequency = 28 c/s).

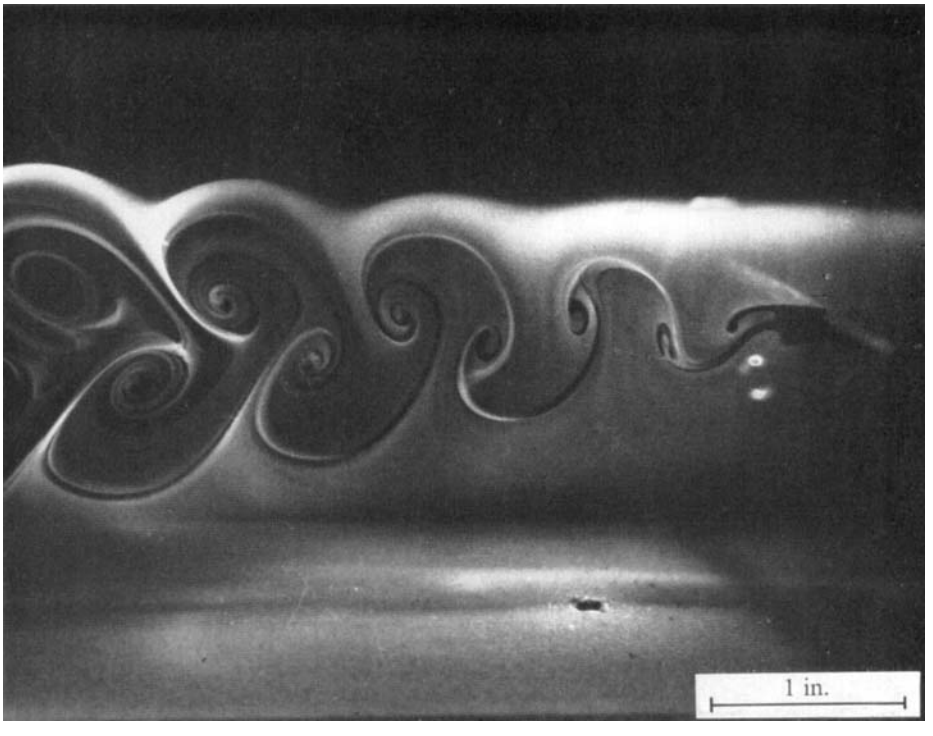

FIGURE 6. Cross-sectional view of vortex wake shedding from a vibrating cylinder (Re = 200, cylinder frequency = 28 c/s).

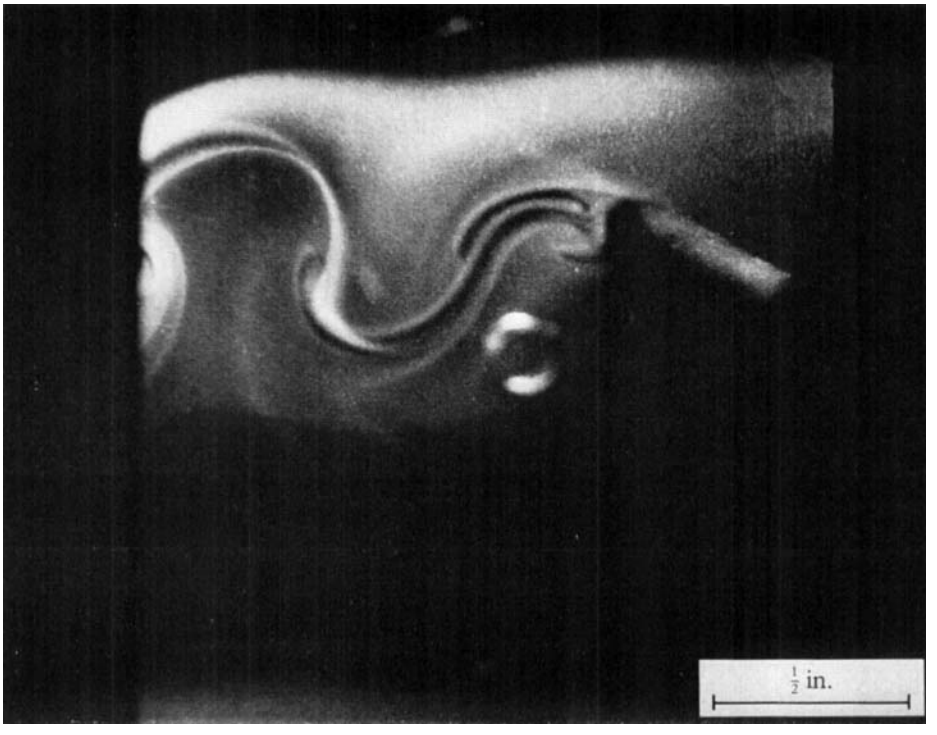

FIGURE 7. The shedding of the early wake with the cylinder at the lowest point of its travel.

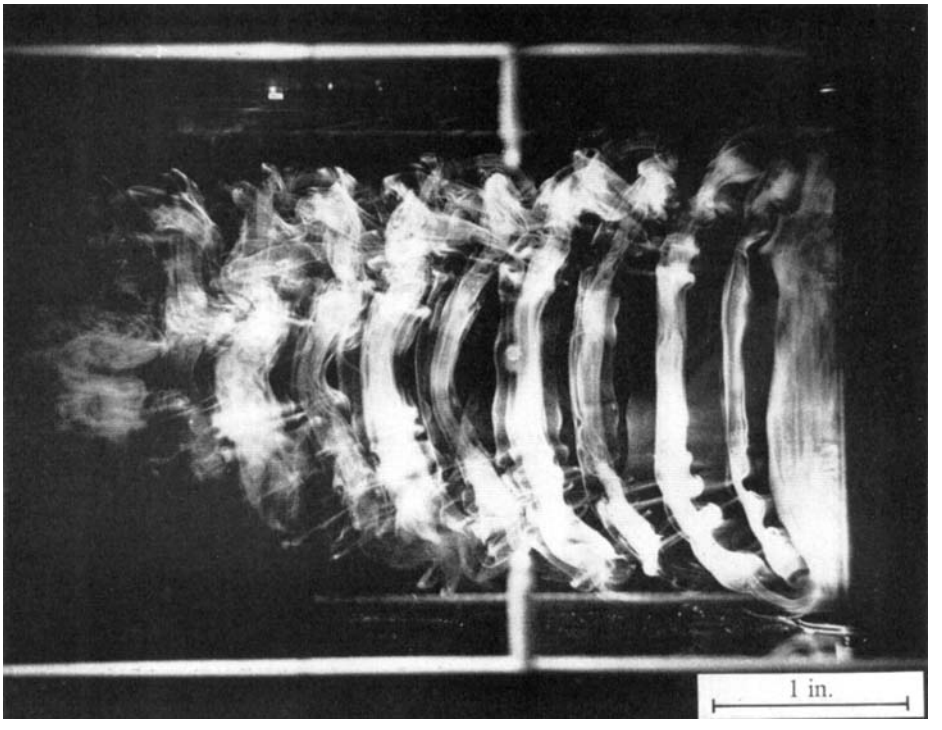

FIGURE 9*a*. Top view of the filaments of a vortex wake shedding from a vibrating cylinder ($Re = 200$, cylinder frequency 32 c/s).

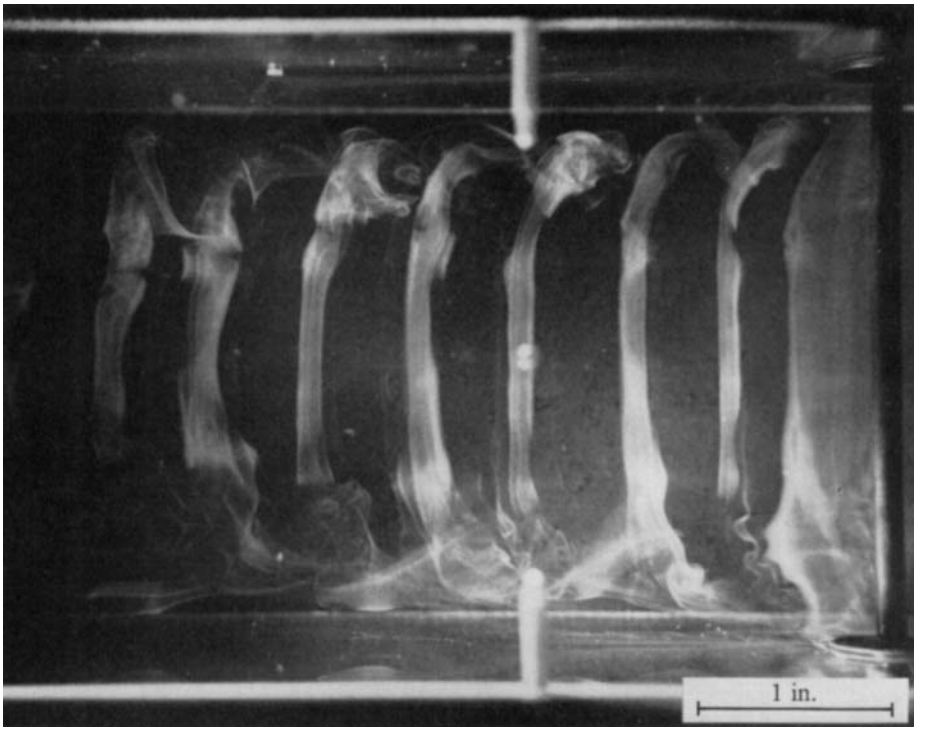

FIGURE 9*b*. Top view of the filaments of a vortex wake shedding from a vibrating cylinder ($Re = 200$, cylinder frequency 24 c/s).

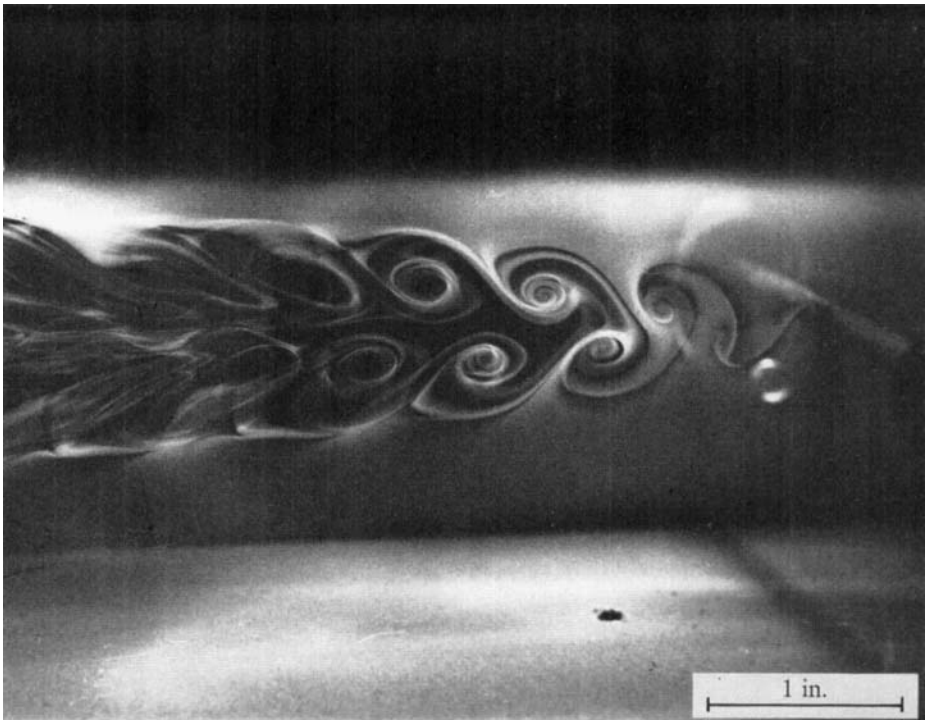

FIGURE 10*a*. Cross-sectional view of the filaments of a vortex wake shedding from a vibrating cylinder (Re = 200, cylinder frequency = 32 c/s).

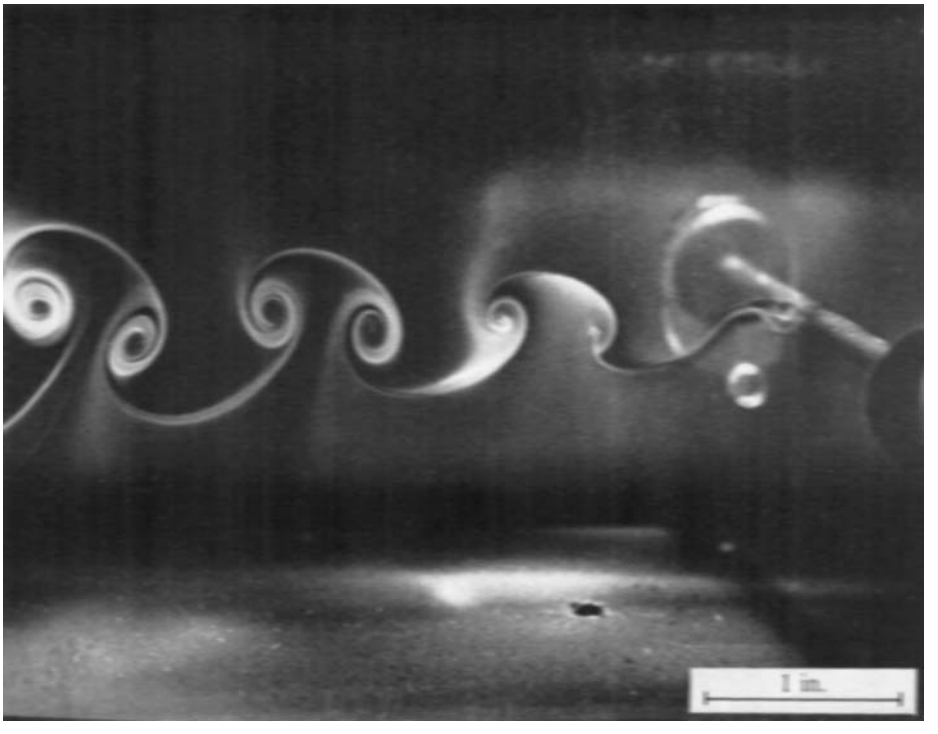

FIGURE 10*b*. Cross-sectional view of the filaments of a vortex wake shedding from a vibrating cylinder (Re = 200, cylinder frequency = 24 c/s).